CRYSTAL GROWTH & DESIGN

Article

Cite This: Cryst. Growth Des. 2019, 19, 1103−1110

pubs.acs.org/crystal

New Methods Versus Old Questions: Crystallization Kinetics of S, Se, and Te

Yimin Chen,[†,‡,§] Rongping Wang,[*,‡] Xiang Shen,[*,‡] Junqiang Wang,[*,§,⊥] and Tiefeng Xu[‡]

[†]Department of Microelectronic Science and Engineering, Faculty of Science and [‡]Laboratory of Infrared Material and Devices & Key Laboratory of Photoelectric Materials and Devices of Zhejiang Province, Advanced Technology Research Institute, Ningbo University, Ningbo 315211, China

[§]CAS Key Laboratory of Magnetic Materials and Devices & Zhejiang Province Key Laboratory of Magnetic Materials and Application Technology, Ningbo Institute of Materials Technology & Engineering, Chinese Academy of Sciences, Ningbo 315201, China

[⊥]Center of Materials Science and Optoelectronics Engineering, University of Chinese Academy of Sciences, Beijing 100049, China

ABSTRACT: Using conventional differential scanning calorimetry (DSC) and Flash DSC, we revisited the old question of crystallization kinetics of chalcogens. Together with the appropriate viscosity models and Stokes−Einstein relation, the quantitative results of crystallization kinetics in chalcogenide supercooled liquids were revealed. It showed that the fragilities of S, Se, Te are 126, 67.5, 60, and the maximum crystal growth rates are 9.7×10^{-3}, 1.3×10^{-6}, and 0.47 m s^{-1} at 0.91, 0.94, and 0.86 T_m, respectively. Such results not only benefit to understand the fundamental science but also help to design new chalcogenide compositions for applications.

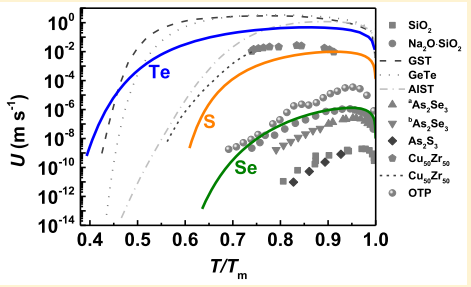

1. INTRODUCTION

Chalcogenide glasses have been used in many fields including biosensing, lithography, optical lenses, waveguides, gratings, and fibers.[1] Recently, ultrafast crystallization kinetics in chalcogenide glasses has made them important in applications of electronic memories and optical recordings.[2] Crystallization kinetics of chalcogenide glasses plays a key role in determining the transport mechanism, thermal stability, and phase transition. Understanding the crystallization mechanism of chalcogenide glasses is essential for the applications mentioned above.

The crystallization kinetics in chalcogenide supercooled liquids is an old topic, which is usually investigated by using either isothermal or non-isothermal method of differential scanning calorimetry (DSC). Compared with the isothermal experiments that are generally time-consuming,[2] the non-isothermal method is frequently employed to investigate the crystallization kinetics. In last decades, the chalcogenides of binary,[3−7] ternary,[2,8−14] and quaternary[1,15,16] were extensively studied by the non-isothermal method. For the crystallization kinetics of elemental chalcogens, selenium (Se) is the most frequently studied due to its low critical cooling rate (R_c), moderate crystallization temperature (T_c) and glass transition temperature (T_g). In the early days, Ryschenkow and Faivre used optical microscope to observe the crystal grain size under isothermal condition and determine the crystal growth rate of Se at the specific temperatures.[17] Recently, Málek et al. showed the results again by IR optical microscope and scanning electron microscope,[18] and further employed the viscosity data around T_g and melting temperature (T_m) to discuss the crystallization kinetics in supercooled Se liquid.[19,20] To our knowledge, however, there is no report on the crystallization kinetics of other two elemental chalcogens, that is, sulfur (S) and tellurium (Te). Only several viscosity data around T_m for S and Te liquids were reported.[21−23]

Quantificational research of elemental chalcogens is significantly important in basic scientific researches. Nevertheless, the lower T_c and higher R_c make it difficult to investigate crystallization kinetics of S and Te by conventional methods. Fortunately, a novel ultrafast calorimetry named Flash DSC, which has been proved successfully to study the crystallization kinetics in chalcogenide phase-change materials, like $Ge_2Sb_2Te_5$ (GST),[24,25] AgIn-Sb_2Te (AIST),[26] Ge−Sb,[27] and GeTe,[28,29] could be a good choice to investigate the crystallization kinetics for elemental chalcogens, since it is featured with wide measurement temperature range (−100 to 450 °C) and ultrafast heating and cooling rates (40 000 and 10 000 K s^{-1}, respectively). In this work, together with the viscosity data and viscosity models, we employed conventional and/or Flash DSC to study the crystallization kinetics of elemental chalcogens. Kinetic parameters achieved from the experiments are useful to design materials for various applications.

Received: October 26, 2018
Revised: December 18, 2018
Published: January 8, 2019

DOI: 10.1021/acs.cgd.8b01608
Cryst. Growth Des. 2019, 19, 1103−1110

2. EXPERIMENTAL METHODS

2.1. Preparation of S Glass. The raw material is crystalline S powder with purity of 99.999 atom % for the preparation of amorphous sulfur. As shown in Figure 1a, we found the melting

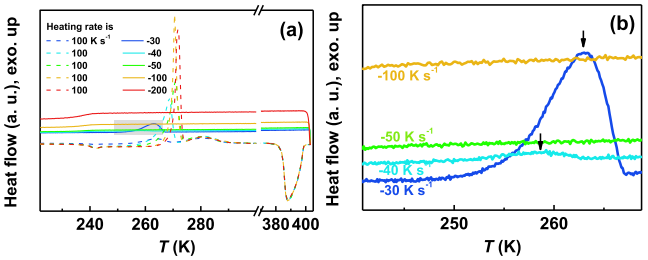

Figure 1. (a) Flash DSC traces for S glass at different cooling rate from 30 to 200 K s^{-1} with the heating rate of 100 K s^{-1}. (b) The enlargement of gray shadow in (a); the arrows indicate the crystallization peaks.

temperature (T_m) was 385 K and the critical cooling rate (R_c) was slightly larger than 30 K s^{-1}. The R_c could be determined clearly in the enlarged view that was shown in Figure 1b, as 50 K s^{-1}. Therefore, in situ preparation of S glass and then the study of its crystallization kinetics became feasible by using Flash DSC.

2.2. Preparation of Se Glass. The raw material is bulk Se with purity of 99.99 atom %. Note that the glass transition temperature (T_g) of Se is very close to room temperature (RT), and its crystallization temperature (T_c) is just slightly higher than RT; these reasons would lead to that amorphous Se crystallizes at RT for a long time. As shown in Figure 2a, we here used X-ray diffraction method to

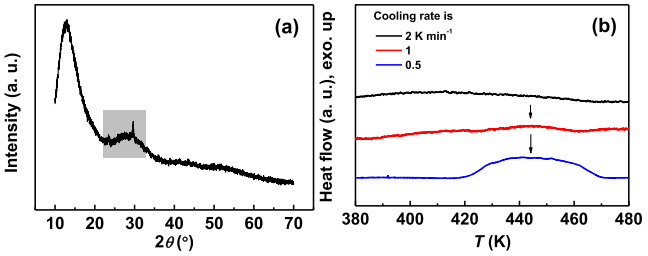

Figure 2. (a) XRD curve of Se element. (b) Conventional DSC traces for Se at different cooling rate.

confirm that Se was partially crystallized. Thus, such raw material should be reamorphized before studying crystallization kinetics. As depicted conventional DSC traces in Figure 2b, it can be seen that the R_c of Se is only 2 K min^{-1}, which indicates both conventional DSC and Flash DSC can be employed to in situ preparation of Se glass and the study of its crystallization kinetics.

2.3. Preparation of Te Glass. The raw material is Te bulk with purity of 99.99 atom %. We used four methods to prepare amorphous Te, including magnetron sputtering, in situ preparation by Flash DSC, single copper roller sling method, and powder spraying method. However, pure amorphous Te cannot be obtained by these four methods due to the ultrahigh R_c (more than 1×10^{10} K s^{-1}) and/or ultralow T_c (near RT) of Te glass. Ultrahigh R_c and ultralow T_c also make it impossible to study crystallization kinetics of Te glass under the present experimental tools. Thus, we here only investigated it by using Stokes−Einstein relation and the viscosity data of Te from the literature.[23]

3. RESULTS

3.1. Crystallization Kinetics of S Glass. Flash DSC was employed to in situ fabricate S glass. The cooling rate is 1000 K s^{-1}, which is higher than the R_c of S glass. Figure 3 showed

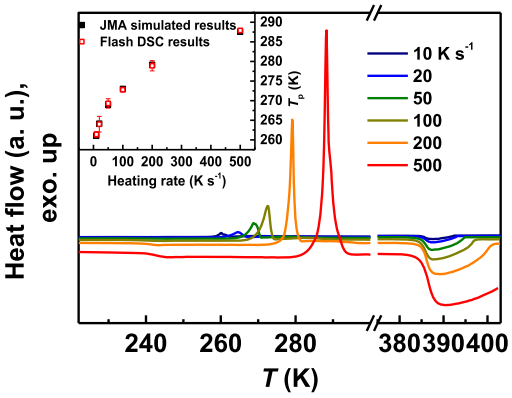

Figure 3. Typical Flash DSC traces of S at different heating rates from 10 to 500 K s^{-1}. (inset) The comparative T_p results from Flash DSC tests and JMA numerical simulations.

the typical Flash DSC traces at different heating rate, that is, 10, 20, 50, 100, 200, and 500 K s^{-1}. The crystallization peak temperature (T_p) increases with increasing heating rate. Henderson confirmed that, with Johnson-Mehl-Avrami (JMA) kinetics, the peak temperature of crystallization on heating in DSC corresponds to a transformed fraction that is always close to 63% ($T_{0.63}$), and this also validates the use of Kissinger method to determine the temperature-dependent crystallization rate.[30] The JMA numerical simulations of DSC peaks for S were performed in this work, and the details could be seen in previous work.[28] The inset of Figure 3 depicts the comparative T_p results of S between Flash DSC tests and JMA numerical simulations. As we can see, the deviation is insignificant even at a high heating rate of 500 K s^{-1}, indicating that T_p values obtained from Flash DSC are all in agreement with $T_{0.63}$. Thus, the data from Flash DSC are viable to depict the crystallization kinetics.

The Kissinger method was performed, and the result was shown in Figure 4a. It can be expressed as[26]

$$\ln(\phi/T_p^2) = -Q/RT_p + A \quad (1)$$

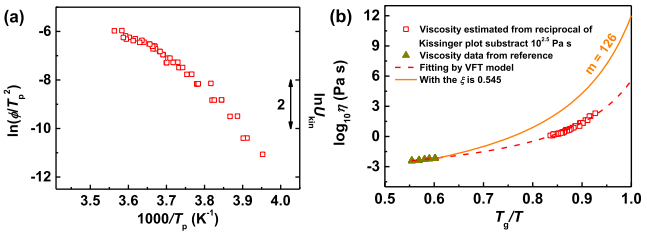

Figure 4. (a) Kissinger plot and relative U_{kin} of S, the data are transformed from T_p values obtained by Flash DSC. (b) Angell plots of S. The red dashed line is fitted by VFT model. The yellow line is the decoupled Angell plot with a decoupling coefficient of 0.545.

where ϕ (K s^{-1}) is heating rate, T_p (K) is peak temperature of crystallization, Q (kJ mol^{-1}) is activation energy for crystallization, R is gas constant as 8.314 J mol^{-1} K^{-1}, and A is a constant. When the heating rate is lower, the obtained Kissinger plot is straight and exhibits an Arrhenius behavior, since Q is considered as a constant. However, once the heating rate becomes higher, it would be curved and exhibits non-Arrhenius behavior with variable Q. Strong non-Arrhenius

DOI: 10.1021/acs.cgd.8b01608
Cryst. Growth Des. 2019, 19, 1103−1110

behavior was revealed in supercooled liquid S by Flash DSC as shown in Figure 4a.

Following Henderson's suggestion,[30] the data depicted in Figure 4a can be considered as relative crystallization kinetics coefficient, U_{kin} (m s^{-1}). Then, the crystal growth rate, U (m s^{-1}) can be extrapolated as[31]

$$U = U_{kin}[1 - \exp(-\Delta G/RT)] \quad (2)$$

where R is the gas constant as mentioned above, and ΔG (kJ mol^{-1}) is the crystallization driving force, which can be expressed as[32,33]

$$\Delta G = \frac{\Delta H_m \Delta T}{T_m}\left(\frac{2T}{T_m + T}\right) \quad (3)$$

where ΔH_m (kJ mol^{-1}) is latent heat of melting, T_m (K) is melting temperature, and ΔT (= $T_m - T$) is the undercooling temperature. On the basis of Stokes–Einstein relation,[32] the relationship between U_{kin} and viscosity η (Pa s) could be obtained as $\eta \propto 1/U_{kin}$, which can be expressed by an equation as

$$\log_{10}\eta = C - \log_{10} U_{kin} \quad (4)$$

where C is a constant, indicating the difference between viscosity and reciprocal of U_{kin}. It can be obtained from adjusting viscosity at T_m (η_{Tm}). We here employed Vogel–Fulcher–Tammann (VFT) viscosity model to account for the temperature-dependent viscosity of supercooled sulfur liquid. The VFT model can be expressed as[34]

$$\log_{10}\eta = \log_{10}\eta_\infty + \frac{A}{T - T_0} \quad (5)$$

where η_∞ (Pa s) is the viscosity at infinite high temperature and A (K) and T_0 (K) are temperature-related parameters, respectively. Thus, we got U_{kin} as

$$\log_{10} U_{kin} = C - \log_{10}\eta_\infty - \left(\frac{A}{T - T_0}\right) \quad (6)$$

As shown in Figure 4b, the hollow data were transported from U_{kin} by using eq 4. The temperature-dependent viscosity data were adjusted by $\eta_{Tm} = 1 \times 10^{-2.17}$ Pa s,[21] and it yields the constant C is 2.5. Then, the red dashed curve in Figure 4b can be fitted by VFT model expressed in eq 5, with the $\eta_\infty = 1 \times 10^{-3.736\ (\pm 0.0705)}$ Pa s, A = 294.3 (±14.76) K, T_0 = 202.9 (±2.27) K, and the fitting degree $R^2 > 0.994$ (it needs to be emphasized we employed the standard T_g of 234.5 K for S glass here). However, it produces a viscosity nearly 6 orders of magnitude lower than the expected $\eta = 1 \times 10^{12}$ Pa s at T_g. Thus, it is necessary to employ the concept of decoupling between U_{kin} and η proposed by Ediger et al. to solve this mismatch.[31] They proposed that the Stokes–Einstein relation would be broken below T_m especially in a fragile supercooled liquid, and the expression of $U_{kin} \propto \eta^{-\xi}$, where ξ is a decoupling coefficient, is more suitable for describing the relation between U_{kin} and η.[31] Here, we used ξ of 0.545 and obtained a new Angell plot as a yellow curve shown in Figure 4b. The fragility of supercooled sulfur liquid can be estimated as $m = [\partial log_{10}\eta/\partial(T_g/T)]_{T=Tg}$,[35] being 126.

With eq 6, the temperature dependence of absolute U_{kin} can be extrapolated as shown in Figure 5a. Together with eqs 2 and 3, and the obtained absolute U_{kin}, ΔH_m (1.962 kJ mol^{-1}), T_m (385 K), the temperature-dependent U can be extrapolated,

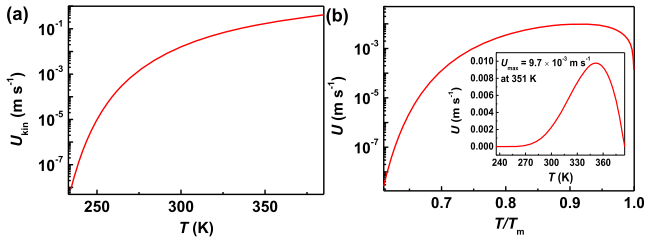

Figure 5. (a) Temperature dependence of absolute U_{kin} for S. (b) Reduced temperature (T/T_m) dependent U for S. (inset) Temperature-dependent U.

and the results are shown in Figure 5b. It yields the maximum crystal growth rate (U_{max}) of 9.7 × 10^{-3} m s^{-1} at 351 K (0.91 T_m).

3.2. Crystallization Kinetics of Se Glass. As we know that T_g and T_c (or T_p) of Se glass are all slightly higher than RT, and the R_c is very low, these conditions make the study of crystallization kientics for Se glass easier compared with other two chalcogens. Ryschenkow et al. and Málek et al. observed the crystal growth rate of Se directly by optical microscope.[17,18] We here employed DSC together with viscosity model to investigate the crystallization kinetics of Se glass. The conventional DSC traces were displayed in Figure 6a with

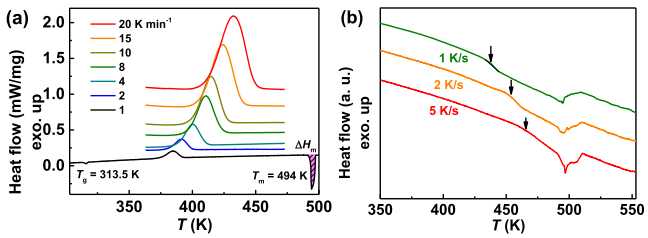

Figure 6. (a) Typical conventional DSC curves for Se; the heating rate is in the range of 1 to 20 K min^{-1}. (b) Typical Flash DSC curves for Se; the heating rate is 1, 2, 5 K s^{-1}, respectively.

heating rates from 1 to 20 K min^{-1}, and the corresponding cooling rate was 20 K min^{-1}. The Flash DSC traces were displayed in Figure 6b with the heating rate of 1, 2, 5 K s^{-1}, respectively, and the corresponding cooling rate is 1 K s^{-1}. All of the cooling traces were not shown here. It can be seen that T_p increases with increased heating rate. From the heating trace of 1 K min^{-1}, T_g, T_m, and ΔH_m can be obtained as 313.5 K, 494 K, and 7.31 kJ mol^{-1}, respectively. As noted in Figure 6b, the crystallization signal in a heating rate of 5 K s^{-1} is weaker than that in a heating rate of 2 K s^{-1}. It implies that the crystallization signal is partially overlapped by melting, which results in inaccurate T_p value in a heating rate of 5 K s^{-1}. Thus, we here only employed T_p measured from Flash DSC with heating rates of 1 and 2 K s^{-1} and conventional DSC with heating rates of 1–20 K min^{-1} to investigate the crystallization kinetics of Se glass.

JMA numerical simulation was performed, but the details were not displayed here. Similar to the analysis for S, the results demonstrated that the Kissinger method can be used to study the crystallization kinetics of Se glass. By using eq 1, the Kissinger plot about Se glass can be performed as shown in Figure 7a. It exhibits a gradual change of the experimental data extracted from conventional and Flash DSC. Using eq 4, we can obtain the transposed viscosity data as red spheres displayed in Figure 7b. It was adjusted by $\eta_{Tm} = 1 \times 10^{0.79}$ Pa s

DOI: 10.1021/acs.cgd.8b01608
Cryst. Growth Des. 2019, 19, 1103–1110

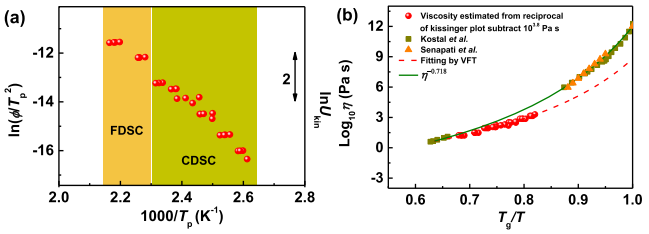

Figure 7. (a) Kissinger plot of Se. (b) Angell plots of Se, the red dashed curve is fitted by VFT model, and the green curve is the decoupled Angell plot with a decoupling coefficient of 0.718.

for Se glass, which yields the constant C is 3.8. They can be perfectly fitted by the VFT viscosity model described in eq 5 with $\eta_\infty = 1 \times 10^{-2.70\ (\pm 0.015)}$ Pa s, A = 854.8 (±2.56) K, and T_0 = 239.6 (±0.49) K. Approximately 4 orders of magnitude lower than the expected $\eta = 1 \times 10^{12}$ Pa s at T_g can be found in this plot. Thus, a decoupling coefficient ξ of 0.718 was employed to adjust this divergence, leading to a new Angell plot as shown in Figure 7b as a green curve. The viscosity result extrapolated from T_p is in good agreement with that reported by Koštál et al.[19] and Senapati et al.[36] Moreover, the estimation of fragility m of supercooled selenium liquid is 67.5, which is close to the values of 61 and 62 reported by Málek et al.[37] and Roland et al.,[38] respectively.

Absolute temperature dependence of U_{kin} was obtained by eq 6, and the result was shown in Figure 8a. Together with the

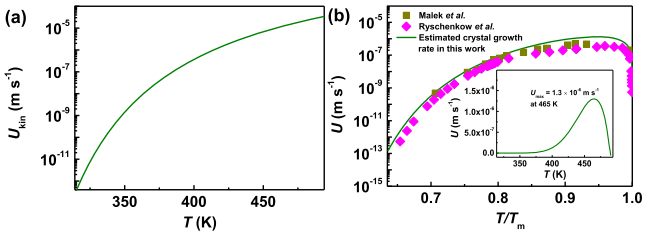

Figure 8. (a) Temperature-dependent absolute U_{kin} of Se. (b) Reduced temperature (T/T_m) dependent crystal growth rate for Se, and the inset is temperature-dependent crystal growth rate. The squares and rhombus represent the crystal growth rate estimated from Ryschenkow et al. and Málek et al., respectively.[17,18]

obtained T_m (494 K) and ΔH_m (7.31 kJ mol^{-1}), temperature-dependent U of Se glass can be extrapolated by eqs 2 and 3. As shown in Figure 8b and its inset, U_{max} for Se glass is 1.3×10^{-6} m s^{-1} at 465 K (0.94 T/T_m). The results in Figure 8b are 2–4 times higher than the crystal growth rates measured by optical microscope from Ryschenkow et al. and Málek et al.[17,18] As we know, spherulitic Se crystal grows up along a- and c-direction. However, Ryschenkow et al.[17] only measured the growth rate along a-direction, because it is difficult to detect the growth rate along c-direction only by optical microscope. The missing crystal growth rate along c-direction in their work leads to an underestimation of total crystal growth rate for Se glass. Obviously, the estimation of crystal growth rate by the DSC method is insensitive to the direction of crystal growth, and thus our result is more reasonable.

3.3. Crystallization Kinetics of Te Glass. Since it was failed to prepare Te glass, the viscosity data were employed to investigate its crystallization kinetics. Fitting the viscosity data reported from Davis[23] by Mauro-Yue-Ellison-Gupta-Allan (MYEGA) viscosity model, the Angell plot of Te glass can

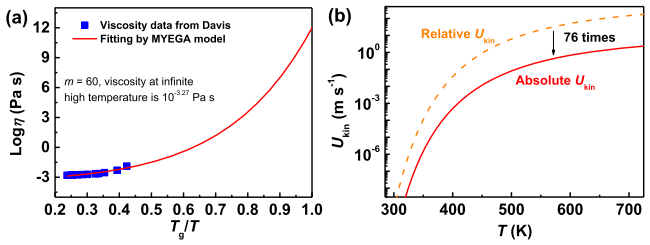

Figure 9. (a) Angell plot and (b) temperature dependence of crystallization kinetics coefficient (U_{kin}) for Te.

be obtained as shown in Figure 9a. The MYEGA model was first proposed by Mauro et al. to describe the viscosity change in supercooled liquid; it can be expressed as[39]

$$\log_{10}\eta = \log_{10}\eta_\infty + (12 - \log_{10}\eta_\infty)\frac{T_g}{T} \times \exp\left[\left(\frac{m}{12 - \log_{10}\eta_\infty} - 1\right)\left(\frac{T_g}{T} - 1\right)\right] \quad (7)$$

where η_∞ (Pa s) is viscosity at infinite high temperature, m is fragility, and T_g (K) is standard glass transition temperature. According to the literature,[40,41] T_g of 285 K was used here for Te. It yields a moderate fragility m of 60 and a reasonable η_∞ of $1 \times 10^{-3.27}$ Pa s.

On the basis of Stokes–Einstein relation ($U_{kin} \propto 1/\eta$), a transposed U_{kin} expression can be obtained as

$$\log_{10}U_{kin} = C' - \log_{10}\eta_\infty - (12 - \log_{10}\eta_\infty)\frac{T_g}{T} \times \exp\left[\left(\frac{m}{12 - \log_{10}\eta_\infty} - 1\right)\left(\frac{T_g}{T} - 1\right)\right] \quad (8)$$

where C' is a constant to indicate the difference between viscosity and reciprocal of U_{kin}. If we ignored the constant ($C' = 0$), a relative U_{kin} can be achieved as shown in the yellow dashed curve in Figure 9b. However, an absolute U_{kin} is prerequisite to understand the crystallization kinetics. Thus, a well estimation of C' is necessary. Orava et al.[24] determined the absolute U_{kin} at T_m for GST by the Stokes–Einstein relation. We here employed the same method to estimate C' and absolute U_{kin}. Together with the relation between diffusive coefficient D (m^2 s^{-1}) and viscosity η (Pa s), $D = kT/3\pi a\eta$, and the relation between U_{kin} and D, $U_{kin} = D/a$, U_{kin} can be derived as

$$U_{kin} = kT/3\pi a^2\eta \quad (9)$$

where k is Boltzmann's constant as 1.38×10^{-23} J K^{-1}, a (nm) is an effective atomic diameter or jump distance. This relation appears to work rather well for high-temperature liquids. With a of 0.3 nm and η of $1 \times 10^{-2.3}$ Pa s at T_m (725 K) for Te, the absolute U_{kin} at T_m can be obtained as 2.333 m s^{-1}. However, the relative U_{kin} at T_m in Figure 9b is 177 m s^{-1}, which is 76 times higher than the absolute value. Therefore, we adjusted the relative U_{kin} to the absolute one that was displayed as red curve in Figure 9b and thus obtained the constant C' of 1.88.

With the conventional DSC, T_m was measured to be 725 K, and ΔH_m was 19.35 kJ mol^{-1} for crystalline Te. Together with

DOI: 10.1021/acs.cgd.8b01608
Cryst. Growth Des. 2019, 19, 1103–1110

these obtained parameters and the absolute U_{kin}, the temperature-dependent crystal growth rate U can be extrapolated by using the eqs 2 and 3. As shown in Figure 10a,b, the maximum crystal growth rate U_{max} is 0.36 m s^{-1} at 640 K (0.89 T_m).

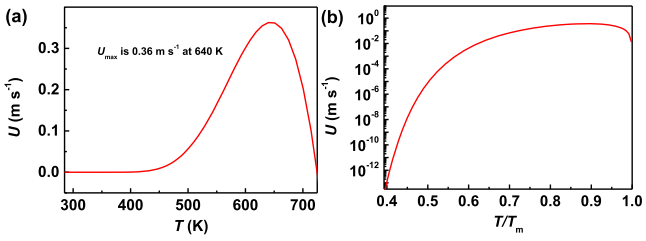

Figure 10. (a) Temperature-dependent crystal growth rate for Te. (b) Reduced temperature-dependent crystal growth rate for Te.

The analyses above did not consider the decouple of Stokes−Einstein relation at lower temperature around T_g for Te glass, which however is important in crystallization kinetics study. Nevertheless, the lack of crystallization and/or viscosity data around T_g limits us to determine this decoupling coefficient in Te supercooled liquid. With the Mossbauer spectrum, the crystallization temperature of amorphous Te was detected to be very close to RT.[41] Therefore, it is reliable to consider that T_p is 300 K at a heating rate of 20 K min^{-1}. By Kissinger method, it yields the relative U_{kin} of 3.7×10^{-6} m s^{-1} at 300 K (hollow start in Figure 11a). Then, an absolute U_{kin} at

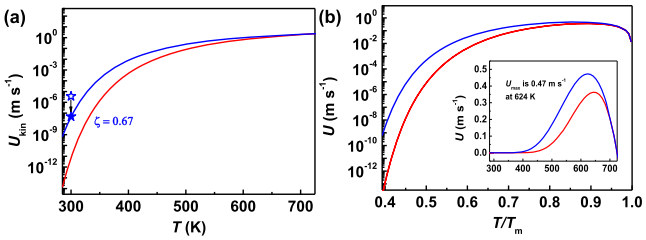

Figure 11. (a) Red and blue curves indicate the temperature dependences of before and after decoupling crystallization kinetics for Te. Hollow and solid start is the relative and absolute U_{kin} at 300 K, respectively. (b) Red and blue curve represents the reduced temperature dependence of before and after decoupling crystal growth rate, respectively.

300 K can be estimated as 4.87×10^{-8} m s^{-1} (solid start in Figure 11a). With the decoupling coefficient ξ of 0.67, a decoupled absolute U_{kin} can be obtained as blue curve through the absolute U_{kin} value at 300 K, and the result is shown in Figure 11a. By using eq 2, the decoupled temperature-dependent U of Te glass is revealed as blue curve depicted in Figure 11b. A significant difference between original and decoupled U (and U_{kin}) is found, especially at a lower temperature range. The inset of Figure 11b shows that the real U_{max} is 0.47 m s^{-1} at 624 K (0.86 T_m).

4. DISSCUSSION

In the paper, the kinetics parameters are basically related only to crystal growth rate, but almost no information on the nucleation rate can be found. Therefore, the role of the nucleation on crystallization kinetics of chalcogens should be elucidated. It is well-known that crystallization kinetics of Se is growth-dominant,[18] and thus the effect of nucleation on the crystallization kinetics is negligible. However, there is no report on whether the crystallization kinetics S and Te is growth- or nucleation-dominant. This could be solved by the isothermal method in the future. Here, we estimated the JMA kinetic exponent (n) close to 1.5 at a temperature of 272 K for S by non-isothermal method, indicating that the nucleation rate would not affect the crystallization at a temperature more than 272 K, which is far from T_{max} of S (351 K). The details for such an estimation are similar to the description in ref 42 and not shown here. For Te, it is believed that a larger amount of vacancies and the weak bond energy in Te clusters make the nucleation easily. Thus, the nucleation would have not much effect on the crystallization for chalcogenide elements in this work.

Table 1 lists the obtained parameters of crystallization kinetics for three chalcogens. We can conclude that all the

Table 1. Obtained Parameters of Crystallization Kinetics for S, Se, Te

glass	η_∞ (Pa s)	U_{max} (m s^{-1})	T_{max}/T_m	T_{rg}	m	ξ
S	$1 \times 10^{-3.73}$	9.7×10^{-3}	0.91	0.609	126	0.545
Se	$1 \times 10^{-2.70}$	1.3×10^{-6}	0.94	0.636	67.5	0.718
Te	$1 \times 10^{-3.27}$	0.47	0.86	0.393	60	0.67

values of η_∞ are converged into the standard value of $1 \times 10^{-2.93}$ Pa s reported by Zheng et al.[43] The value of U_{max} is maximum for Te and minimum for Se with the difference of ~2 to 3 orders of magnitude in each other. The lower U_{max} is, the larger reduced temperature T_{max}/T_m is, which follows the normal rule concluded by Orava et al.[44] Moreover, the relation between U_{max} and T_{rg} is in agreement with the empirical rule suggested by Chen et al.[45] The relation between fragility m and decoupling coefficient ξ for the chalcogens was displayed in Figure 12. It is evident that the present results are roughly in line with the relation reported by Ediger et al.,[31] $\xi \approx 1.1-0.005m$, as shown the red line in Figure 12.

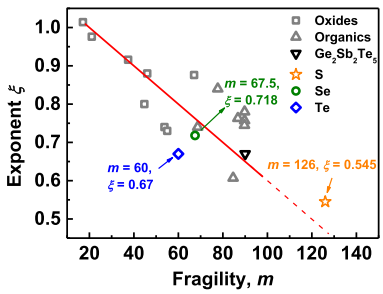

Figure 12. Relation between fragility m and decoupling coefficient ξ.

Figure 13 shows the reduced temperature (T/T_m) dependent crystal growth rate for different materials, including oxide, organic, metallic, and chalcogenide glasses. The obtained data of S, Se, and Te in this work are also displayed in Figure 13. As we know, phase-change materials, such as conventional GST,[24] GeTe,[28] AgIn-Sb_2Te (AIST),[26] and so on, are generally Te based, due to their fast crystallization kinetics. The addition of the elements such as Ge, Sb, and others, into Te-based materials could accelerate the crystal growth rate around T_m but reduce it near T_g. The properties with fast crystallization speed at high temperature and good thermal stability at low temperature are essential for phase-change materials. The fast

DOI: 10.1021/acs.cgd.8b01608
Cryst. Growth Des. 2019, 19, 1103−1110

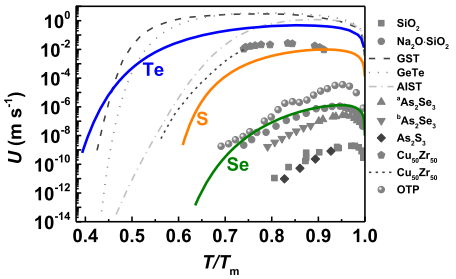

Figure 13. Reduced temperature (T/T_m) dependent crystal growth rate for different materials. All the crystal growth rates of SiO_2, $Na_2O{\cdot}SiO_2$, $Cu_{50}Zr_{50}$, OTP,[44] and GST,[24] GeTe,[28] AIST,[26] as well as As_2Se_3[52,53] are obtained from the literature. The crystal growth rates of As_2S_3 (black rhombuses) at standard atmospheric pressure (~100 kPa) were estimated from the data measured at an ultrahigh pressure of 15 kbr.[54]

crystallization kinetics of Te makes it difficult to form bulk glasses via the conventional water-cooling method, although the doping of good glass elements like As could improve the glass-forming ability.

The crystal growth rate in Se glass is faster than that in SiO_2, slower than that in *o*-terphenyl (OTP), and close to that in $Na_2O{\cdot}SiO_2$. The large T_{rg} (0.636) implies that Se is a good glass former. Se-based materials are easily formed into bulk glasses with different dopant of Ge, As, and others, and they are always the first choice to prepare the bulk chalcogenides. As depicted in Figure 13, the crystal growth rate in As_2Se_3 is lower, and T_{rg} is larger apparently when As is introduced into Se matrix. In contrast, it does not encourage Se as the base material for phase-change application, but appropriate doping can enhance the thermal stability greatly.[46]

It is highly desired that the crystallization in glass is controllable. Among three chalcogens, S glass possesses moderate crystal growth rate, that is, slightly lower than the typical metallic glass $Cu_{50}Zr_{50}$. The moderate growth rate makes it a good candidate to create glass-ceramic in S-based glasses like Ge−S[47,48] and Ge−Ga−S.[49,50] Doping nonmetallic element into S matrix can obtain good glass former, for example, As_2S_3, which has an ultralow crystal growth rate (black rhombuses in Figure 13). This makes As_2S_3 an excellent material for optical lens and fiber. Although sulfur was also considered as one of the compositions for phase-change material in early time,[51] its submicron crystal growth rate cannot meet current requirement for phase-change memory.

Although crystallization kinetics of three chalcogen elements exhibit different behaviors, and this has substantial implication on the crystallization kinetics of multicomponent chalcogenide glasses based on three chalcogen elements, we also can see that crystallization kinetics of a multicomponent chalcogenide could be very different from that of a single-element chalcogen from Figure 13. For example, crystal growth of As_2S_3 glass is so much slower than S glass, even slower than Se glass, while Ge−S and Ge−Ga−S glasses may exhibit relatively much faster crystal growth. This indicates that the crystal growth rates could range very broadly among S-based glasses, and competitive factors from other glass-forming elements such as Ge, Ga, and so on could affect the crystal growth rates greatly. However, the present study does not intend to categorize and compare their crystal growth rates just in terms of relative crystal growth rates of chalcogen elements. Although it is well-accepted that Te-based glasses have a faster crystallization rates and thus the glass community generally search materials with fast crystallization rate based on Te-glasses, it is also possible to tune crystallization rate using suitable glass-forming elements.

Previously, Jones et al. used molecular dynamics and density functional approaches to study the ground state geometries of sulfur and selenium clusters.[55,56] Such investigation was also performed on amorphous tellurium recently.[57] It was found that the chains in amorphous Te are shorter than those in S and Se, and the threefold-coordinated Te atoms can be located at the branches. Mostly, it was claimed that ~37% of total volume as the cavities are presented in amorphous Te, but this has not been reported in amorphous S and Se.[57] A mass of cavities can help to realize the fast crystallization speed in amorphous Te that is also the characteristic in Te-based phase-change materials.[58]

5. CONCLUSIONS

The conventional and Flash DSC were performed to study the crystallization kinetics of elemental chalcogens, that is, S, Se, and Te. Together with viscosity model, the temperature dependences of U_{kin}, η, and U were extrapolated. It was found that their viscosities at infinite high temperature are convergent to the standard value of $1 \times 10^{-2.93}$ Pa s, and the relation between fragility (m) and decoupling coefficient (ξ) roughly follows Ediger's experimental equation, that is, $\xi \approx 1.1-0.005m$. These verify the reliability of the present study of crystallization kinetics for three elemental chalcogens. The maximum crystal growth rates of S, Se, and Te are 9.7×10^{-3}, 1.3×10^{-6}, and 0.47 m s^{-1} at 0.91 T_m, 0.94 T_m, and 0.86 T_m, respectively. Compared to other glasses, we found that these three elemental chalcogens have slow (Se), moderate (S), and fast (Te) crystallization kinetics, respectively. Slow crystallization kinetics makes Se a good choice for glass matrix, moderate crystallization kinetics makes S a candidate for glass-ceramic matrix, while the fast crystallization kinetics in Te makes it more suitable as the base material for phase-change memory.

AUTHOR INFORMATION

Corresponding Authors

*E-mail: wangrongping@nbu.edu.cn. (R.W.)
*E-mail: shenxiang@nbu.edu.cn. (X.S.)
*E-mail: jqwang@nimte.ac.cn. (J.W.)

ORCID

Yimin Chen: 0000-0002-3057-5062

Notes

The authors declare no competing financial interest.

ACKNOWLEDGMENTS

This work was financially supported by the Natural Science Foundation of China (Grant Nos. 61775111, 61775109, and 51771216), Zhejiang Provincial Natural Science Foundation of China (LR18E010002), international cooperation project of Ningbo City (Grant No. 2017D10009), 3315 Innovation Team in Ningbo City, One Hundred Talents Program of Chinese Academy of Sciences, and sponsored by K. C. Wong Magna Fund in Ningbo Univ.

REFERENCES

(1) Kumar, A.; Fouad, S. S.; El-Bana, M. S.; Mehta, N. Thermal analysis of cadmium addition on the glass transition and

DOI: 10.1021/acs.cgd.8b01608
Cryst. Growth Des. 2019, 19, 1103−1110

crystallization kinetics of Se-Te-Sn glassy network. *J. Therm. Anal. Calorim.* **2018**, *131*, 2491−2501.
(2) Atyia, H. E.; Farid, A. S. Non-isothermal crystallization kinetics of ternary $Se_{90}Te_{10-x}Pb_x$ glasses. *J. Cryst. Growth* **2016**, *436*, 125−133.
(3) Svoboda, R.; Brandová, D.; Málek, J. Non-isothermal crystallization kinetics of $GeTe_4$ infrared glass. *J. Therm. Anal. Calorim.* **2016**, *123*, 195−204.
(4) Svoboda, R.; Málek, J. Kinetic fragility of Se-based binary chalcogenide glasses. *J. Non-Cryst. Solids* **2015**, *419*, 39−44.
(5) Joraid, A. A.; Abu El-Oyoun, M.; Afify, N. Phase separation and crystallization kinetics studies of amorphous $Si_{10}Te_{90}$. *Chalcogenide Lett.* **2016**, *13*, 79−89.
(6) Abdel-Rahim, M. A.; Hafiz, M. M.; Abdel-Latief, A. Y.; Abd-Elnaiem, A. M.; Alwany, A. E. B. A study of the non-isothermal crystallization kinetic of $Zn_{10}Se_{90}$ glass. *Appl. Phys. A: Mater. Sci. Process.* **2015**, *119*, 881−890.
(7) Svoboda, R.; Málek, J. Non-isothermal crystallization kinetics of As_2Se_3 glass studied by DSC. *Thermochim. Acta* **2014**, *579*, 56−63.
(8) Khan, S. A.; Zulfequar, M.; Husain, M. On the crystallization kinetics of amorphous $Se_{80}In_{20-x}Pb_x$. *Solid State Commun.* **2002**, *123*, 463−468.
(9) Vazquez, J.; Wagner, C.; Villares, P.; Jiménez-Garay, R. Glass transition and crystallization kinetics in $Sb_{0.18}As_{0.34}Se_{0.48}$ glassy alloy by using non-isothermal techniques. *J. Non-Cryst. Solids* **1998**, *235−237*, 548−553.
(10) Mahmoud, A. Z.; Mohamed, M.; Moustafa, S.; Abdelraheem, A. M.; Abdel-Rahim, M. A. Study of non-isothermal crystallization kinetics of $Ge_{20}Se_{70}Sn_{10}$ chalcogenide glass. *J. Therm. Anal. Calorim.* **2018**, *131*, 2433−2442.
(11) Mohamed, M.; Abd-el Salam, M. N.; Abdel-Rahim, M. A.; Abdel-Latief, A. Y.; Shaaban, E. R. Effect of Ag addition on crystallization kinetics and thermal stability of As−Se chalcogenide glasses. *J. Therm. Anal. Calorim.* **2018**, *132*, 91−101.
(12) El-sonbaty, S. S.; Abd-Elrahman, M. I.; Abu-Sehly, A. A.; Hafiz, M. M. Thermal stability, glass transition and crystallization kinetics of $Se_{95-x}Sb_5In_x$ chalcogenide. *Appl. Phys. A: Mater. Sci. Process.* **2018**, *124*, 186.
(13) Svoboda, R.; Brandová, D. The effect of powder coarseness on crystallization kinetics of $Ge_{11}Ga_{11}Te_{78}$ infrared glass. *J. Therm. Anal. Calorim.* **2017**, *129*, 593−599.
(14) Fernandes, B. J.; Naresh, N.; Ramesh, K.; Sridharan, K.; Udayashankar, N. K. Crystallization kinetics of Sn doped $Ge_{20}Te_{80-x}Sn_x$ ($0 \leq x \leq 4$) chalcogenide glassy alloys. *J. Alloys Compd.* **2017**, *721*, 674−682.
(15) Sharda, S.; Sharma, N.; Sharma, P.; Sharma, V. Thermal stability and crystallization kinetics of quaternary Sb-Se-Ge-In chalcogenide glasses. *J. Alloys Compd.* **2014**, *611*, 96−99.
(16) Kaistha, A.; Modgil, V.; Rangra, V. S. Calorimetric study of Sb-modified Ge-Se-Te glassy alloys. *J. Therm. Anal. Calorim.* **2017**, *129*, 1323−1331.
(17) Ryschenkow, G.; Faivre, G. Bulk crystallization of liquid selenium Primary nucleation, growth kinetics and modes of crystallization. *J. Cryst. Growth* **1988**, *87*, 221−235.
(18) Málek, J.; Barták, J.; Shánělová, J. Spherulitic crystal growth velocity in Selenium supercooled liquid. *Cryst. Growth Des.* **2016**, *16*, 5811−5821.
(19) Koštál, P.; Hofírek, T.; Málek, J. Viscosity measurement by thermomechanical analyzer. *J. Non-Cryst. Solids* **2018**, *480*, 118−122.
(20) Koštál, P.; Málek, J. Viscosity of selenium melt. *J. Non-Cryst. Solids* **2010**, *356*, 2803−2806.
(21) Gee, G. The molecular complexity of sulphur in the liquid and vapour. *Trans. Faraday Soc.* **1952**, *48*, 515−526.
(22) Sagan, C. Sulphur flows on Io. *Nature* **1979**, *280*, 750−753.
(23) Davis, E. A. *Electronic and Structural Properties of Amorphous Semiconductors;* Le Comber, P. G., Mort, J., Eds.; Academic Press: New York, 1973.
(24) Orava, J.; Greer, A. L.; Gholipour, B.; Hewak, D. W.; Smith, C. E. Characterization of supercooled liquid $Ge_2Sb_2Te_5$ and its crystallization by ultrafast-heating calorimetry. *Nat. Mater.* **2012**, *11*, 279−283.
(25) Chen, B.; ten Brink, G. H.; Palasantzas, G.; Kooi, B. J. Crystallization kinetics of GeSbTe phase-change nanoparticles resolved by ultrafast calorimetry. *J. Phys. Chem. C* **2017**, *121*, 8569−8578.
(26) Orava, J.; Hewak, D. W.; Greer, A. L. Fragile-to-strong crossover in supercooled liquid Ag-In-Sb-Te studied by ultrafast calorimetry. *Adv. Funct. Mater.* **2015**, *25*, 4851−4858.
(27) Chen, B.; Momand, J.; Vermeulen, P. A.; Kooi, B. J. Crystallization kinetics of supercooled liquid Ge−Sb based on ultrafast calorimetry. *Cryst. Growth Des.* **2016**, *16*, 242−248.
(28) Chen, Y.; Wang, G.; Song, L.; Shen, X.; Wang, J.; Huo, J.; Wang, R.; Xu, T.; Dai, S.; Nie, Q. Unraveling the crystallization kinetics of supercooled liquid GeTe by ultrafast calorimetry. *Cryst. Growth Des.* **2017**, *17*, 3687−3693.
(29) Chen, B.; de Wal, D.; Ten Brink, G. H.; Palasantzas, G.; Kooi, B. J. Resolving Crystallization Kinetics of GeTe Phase-Change Nanoparticles by Ultrafast Calorimetry. *Cryst. Growth Des.* **2018**, *18*, 1041−1046.
(30) Henderson, D. W. Thermal analysis of non-isothermal crystallization kinetics in glass forming liquids. *J. Non-Cryst. Solids* **1979**, *30*, 301−315.
(31) Ediger, M.; Harrowell, P.; Yu, L. Crystal growth kinetics exhibit a fragility-dependent decoupling from viscosity. *J. Chem. Phys.* **2008**, *128*, 034709.
(32) Thompson, C. V.; Spaepen, F. On the approximation of the free energy change on crystallization. *Acta Metall.* **1979**, *27*, 1855−1859.
(33) Battezzati, L.; Greer, A. Thermodynamics of $Te_{80}Ge_{20-x}Pb_x$ glass-forming alloys. *J. Mater. Res.* **1988**, *3*, 570−575.
(34) Scherer, G. W. Editorial comments on a paper by Gordon S. Fulcher. *J. Am. Ceram. Soc.* **1992**, *75*, 1060−1062.
(35) Angell, C. A. Glass-formers and viscous liquid slowdown since David Turnbull: enduring puzzles and new twists. *MRS Bull.* **2008**, *33*, 544−555.
(36) Senapati, U.; Varshneya, A. K. Viscosity of chalcogenide glass-forming liquids: an anomaly in the 'strong' and 'fragile' classification. *J. Non-Cryst. Solids* **1996**, *197*, 210−218.
(37) Málek, J.; Svoboda, R.; Pustková, P.; Čičmanec, P. Volume and enthalpy relaxation of a-Se in the glass transition region. *J. Non-Cryst. Solids* **2009**, *355*, 264−272.
(38) Roland, C. M.; Santangelo, P. G.; Plazek, D. J.; Bernatz, K. M. Creep of selenium near the glass temperature. *J. Chem. Phys.* **1999**, *111*, 9337−9342.
(39) Mauro, J. C.; Yue, Y.; Ellison, A. J.; Gupta, P. K.; Allan, D. C. Viscosity of glass-forming liquids. *Proc. Natl. Acad. Sci. U. S. A.* **2009**, *106*, 19780−19784.
(40) Donald, I. W.; Davies, H. A. Prediction of glass-forming ability for metallic systems. *J. Non-Cryst. Solids* **1978**, *30*, 77−85.
(41) Blum, N. A.; Feldman, C. Mössbauer study of amorphous and crystalline tellurium. *Solid State Commun.* **1974**, *15*, 965−968.
(42) Kong, L. H.; Gao, Y. L.; Song, T. T.; Wang, G.; Zhai, Q. J. Non-isothermal crystallization kinetics of FeZrB amorphous alloy. *Thermochim. Acta* **2011**, *522*, 166−172.
(43) Zheng, Q.; Mauro, J. C.; Ellison, A. J.; Potuzak, M.; Yue, Y. Universality of the high-temperature viscosity limit of silicate liquids. *Phys. Rev. B: Condens. Matter Mater. Phys.* **2011**, *83*, 212202.
(44) Orava, J.; Greer, A. Fast and slow crystal growth kinetics in glass-forming melts. *J. Chem. Phys.* **2014**, *140*, 214504.
(45) Chen, Y.; Pan, H.; Mu, S.; Wang, G.; Wang, R.; Shen, X.; Wang, J.; Dai, S.; Xu, T. Intermediate crystallization kinetics in Germanium-Tellurides. *Acta Mater.* **2019**, *164*, 473−480.
(46) Chen, Y.; Wang, G.; Tian, M.; Shen, X.; Xu, T.; Lu, Y.; Dai, S.; Nie, Q. Fast reversible laser-induced crystallization of Sb-rich Zn-Sb-Se phase change material with excellent stability. *AIP Adv.* **2015**, *5*, 077174.
(47) Lin, C.; Tao, H.; Wang, Z.; Wang, B.; Zang, H.; Zheng, X.; Zhao, X. Defect configurations in Ge-S chalcogenide glasses studied

DOI: 10.1021/acs.cgd.8b01608
Cryst. Growth Des. 2019, 19, 1103−1110

by Raman scattering and positron annihilation technique. *J. Non-Cryst. Solids* **2009**, *355*, 438−440.
(48) Lin, C.; Tao, H.; Zheng, X.; Pan, R.; Zang, H.; Zhao, X. Second-harmonic generation in IR-transparent β-GeS_2 crystallized glasses. *Opt. Lett.* **2009**, *34*, 437−439.
(49) Wang, R.; Yan, K.; Zhang, M.; Shen, X.; Dai, S.; Yang, X.; Yang, Z.; Yang, A.; Zhang, B.; Luther-Davies, B. Chemical environment of rare earth ions in $Ge_{28.125}Ga_{6.25}S_{65.625}$ glass-ceramics doped with Dy^{3+}. *Appl. Phys. Lett.* **2015**, *107*, 161901.
(50) Yang, X.; Zhang, M.; Yan, K.; Han, L.; Xu, Q.; Liu, H.; Wang, R. Controllable formation of the crystalline phases in Ge-Ga-S chalcogenide glass-ceramics. *J. Am. Ceram. Soc.* **2017**, *100*, 74−80.
(51) Feinleib, J.; deNeufville, J.; Moss, S. C.; Ovshinsky, S. R. Rapid reversible light-induced crystallization of amorphous semiconductors. *Appl. Phys. Lett.* **1971**, *18*, 254−257.
(52) Málek, J.; Shánělová, J.; Martinková, S.; Pilný, P.; Koštál, P. Crystal Growth Velocity in As_2Se_3 Supercooled Liquid. *Cryst. Growth Des.* **2017**, *17*, 4990−4999.
(53) Henderson, D. W.; Ast, D. G. Viscosity and crystallization kinetics of As_2Se_3. *J. Non-Cryst. Solids* **1984**, *64*, 43−70.
(54) Devaud, G.; Aziz, M. J.; Turnbull, D. High-pressure crystallization kinetics of As_2S_3. *J. Non-Cryst. Solids* **1989**, *109*, 121−128.
(55) Hohl, D.; Jones, R. O.; Car, R.; Parrinello, M. Structure of sulfur clusters using simulated annealing: S_2 to S_{13}. *J. Chem. Phys.* **1988**, *89*, 6823−6835.
(56) Hohl, D.; Jones, R. O.; Car, R.; Parrinello, M. The structure of selenium clusters-Se_3 to Se_8. *Chem. Phys. Lett.* **1987**, *139*, 540−545.
(57) Akola, J.; Jones, R. O. Structure and dynamics in amorphous Tellurium and tenclusters: A density functional study. *Phys. Rev. B: Condens. Matter Mater. Phys.* **2012**, *85*, 134103.
(58) Akola, J.; Jones, R. O. Structural phase transitions on the nanoscale: The crucial pattern in the phase-change materials $Ge_2Sb_2Te_5$ and GeTe. *Phys. Rev. B: Condens. Matter Mater. Phys.* **2007**, *76*, 235201.

DOI: 10.1021/acs.cgd.8b01608
Cryst. Growth Des. 2019, 19, 1103−1110